Int. J. Impact Engng Vol.14, pp.763–774, 1993
Printed in Great Britain

0734-743X/93 $6.00+0.00

A HYPERVELOCITY FRAGMENT LAUNCHER BASED ON AN INHIBITED SHAPED CHARGE

JAMES D. WALKER, DONALD J. GROSCH, and SCOTT A. MULLIN

Southwest Research Institute
San Antonio, Texas 78228-0510

ABSTRACT

A hypervelocity fragment launcher based on an inhibited shaped charge was developed, which launches a 0.5-1.0 g aluminum fragment at 11.2±0.2 km/s. Experimental and computational work performed during its development are presented. The launched fragment is characterized by in-flight flash radiography and impact crater examination.

INTRODUCTION

Impacts on spacecraft and satellites from orbiting debris in space are a growing concern, due to the amount of debris and the potentially high impact velocities. Low Earth orbital velocity ranges from 7.3 to 7.8 km/s. Space Station Freedom will have an orbital velocity near 7.7 km/s (NASA, 1991). Debris in orbits with differing inclination angles, but similar heights, have similar velocities. If α is the difference in inclination angle between two intersecting orbits, then the impact velocity is given by

$$v_{impact} = \sqrt{2 - 2\cos\alpha}\, v_{orbit} \tag{1}$$

A collision between a spacecraft and debris in polar and equatorial orbits ($\alpha = 90°$) would occur at a velocity of 10.9 km/s for $v_{orbit} = 7.7$ km/s, while a collision between a spacecraft and debris in standard and retrograde orbits ($\alpha = 180°$) would occur at 15.4 km/s. Thus, to test shielding concepts for spacecraft, it is necessary to perform laboratory impact tests in the 11 to 15 km/s regime. Two-stage light gas guns are able to launch projectiles at speeds up to 9 km/s. To launch projectiles at higher velocities, we began examining explosive launching techniques.

Metal lined shaped charges are able to produce metal jets with tip speeds over 10 km/s. In the 1960's, the concept of using a shaped charge and severing the high velocity jet to isolate the jet tip as a fragment was investigated (Kronman and Merendino, 1963, Merendino, *et al.*, 1963, Wenzel and Gehring, 1965, Wenzel, 1986). However, a series of recent tests revealed limitations of the previous work (Tullos, *et al.*, 1988). An experimental and computational modeling program was initiated to re-examine the concept and attempt to design a hypervelocity fragment launcher based on an inhibited shaped charge.

This paper first presents a brief overview of shaped charge jets to suggest the possible applicability and performance of an explosive fragment launching device. Experimental and computational results are then presented to provide information on the liner collapse process; this information was used in the design of the charge. The simulations were not sufficiently accurate to perform the complete design on the computer, due as much to a lack of material response information at the extreme pressures and strain rates involved as to numerical inaccuracies. Also, the simulations were two dimensional, and the final charge design was three dimensional, having asymmetric components. During the design process, there was a strong interplay between the experimental work and computational work, both of which led to a conceptual understanding of the collapse and subsequent jet-inhibitor interaction. Numerous experimental tests and the synergism between the experiments and the computations led to an understanding of the device and a working hypervelocity fragment launcher.

The launched aluminum fragment has a length to diameter ratio (L/D) between 3 and 4, with a nominal diameter of 5 mm. Its mass ranges from 0.5 to 1.0 gram. Occasionally, the fragment rotates in flight, which led to a confirmation that the fragment is hollow. The velocity of the fragment is 11.2±0.2 km/s. At the end of the article, flash radiographs of the fragment and a photograph of a crater produced in a large aluminum target are presented.

THE SHAPED CHARGE APPROACH

Shaped Charges

The explosively driven collapse of a metal lined cavity produces a high velocity metal jet of relatively great length (for an overview of shaped charges, see Walters and Zukas, 1989). For shielding analysis, a high velocity fragment with an L/D = 1 would be ideal. To take advantage of the high velocities produced by shaped charges, it is necessary to isolate a fragment at the leading tip of the jet.

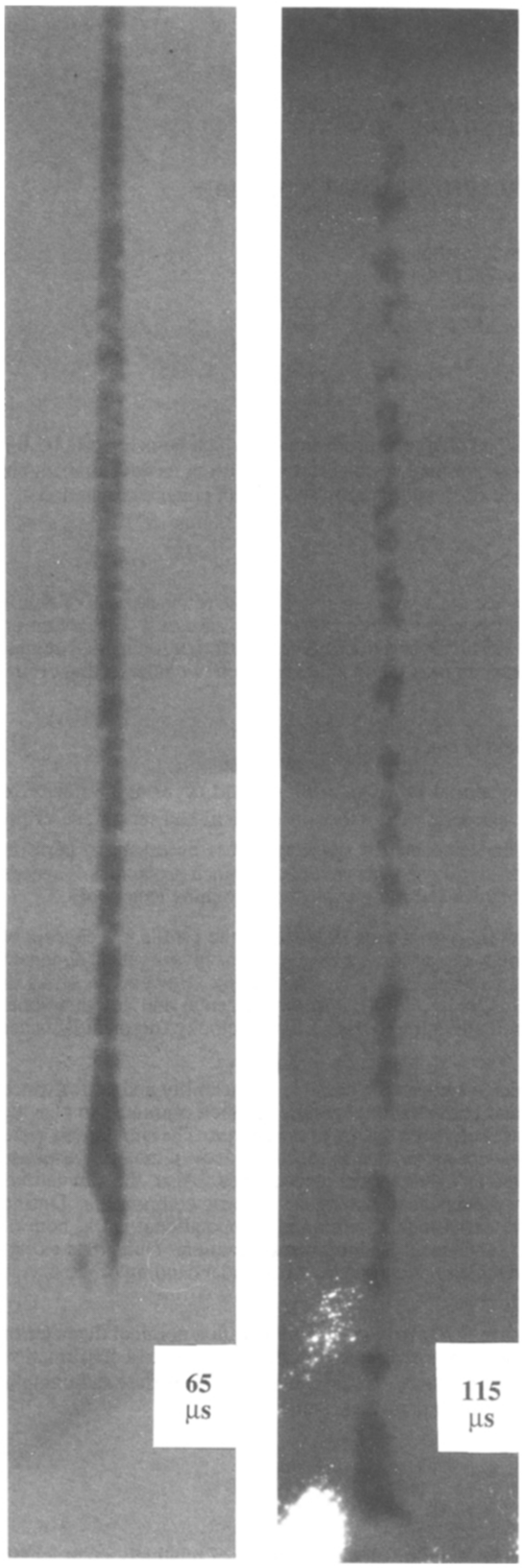

Fig. 1. X-ray views from an aluminum 30° liner angle charge. The left figure at 65 μs after detonation of the charge shows the intact jet, and the right figure at 115 μs shows the fragmenting jet.

The long jet formed by the shaped charge has a large velocity gradient. This gradient eventually causes the jet to break into small fragments. Figure 1 shows a portion of an aluminum jet from a 30° conical shaped charge whose explosive component was Octol 70/30. The jet tip is travelling at 11.1 km/s. The left frame, at 65 μs after initiation, shows the long stretching jet and the second frame, at 115 μs, shows the jet shortly after breaking into fragments. The fragments have an L/D ranging from 1 to 5. The large jet tip is evident.

The high speed leading fragment of the jet would be an excellent projectile for hypervelocity impact testing. To remove the unwanted trailing fragments, material is placed within the cavity of the shaped charge. This material inhibits the formation of the majority of the jet, and hence will be referred to as an "inhibitor." The inhibitor allows the jet tip to form, but removes most of following jet material. Only the leading fragment is allowed to travel down the flight line.

Jet Incoherence and Expected Velocities

It has been observed that in some shaped charge jets there is a large radial component to the jet velocity, resulting in a radial expansion of the jet material as it travels down range. This is referred to as incoherence of the jet. For example, Fig. 2 shows the tip of an aluminum jet for a 20° liner angle with Octol 70/30 explosive. The jet tip is travelling at 12.0 km/s, but is undergoing radial expansion (this result for aluminum agrees with that of Kronman and Merendino, 1963). An incoherent jet will not produce a desirable fragment for space debris simulation, since it is breaking into many pieces.

A large amount of research has been performed on jet incoherence. In general, there seems to be a jet tip velocity below which the jet is coherent, and above which it is not (Walters and Zukas, 1989, Chanteret, 1992). This velocity depends on the liner material and the shape of the cavity (for example, the liner angle for a conical charge). Different jet tip velocities for a given material can be achieved by using different cavity geometries and explosives with different detonation velocities.

A starting place for the design of a hypervelocity launcher is the charge with the highest jet tip velocity for a coherent jet. An exact analytical expression for the maximum coherent jet tip velocity has not been found, and so charge designers use empirical expressions to estimate this quantity. Most of these expressions compare the velocity at which the liner material is moving into the collapse region with the sound speed of the material. One such expression is

$$V_l \leq 1.23 c_0 \tag{2}$$

In this equation V_l is the velocity at which the liner material is moving into the collapse region and c_0 is usually taken to be the bulk sound speed of the liner material. A heuristic interpretation of this equation is that the flow must be subsonic: the collapse velocity V_l must be less than the sound speed of the highly compressed material in the vicinity of the collapse point (hence, the 1.23 factor). This expression seems to hold for a number of materials, where V_l is obtained from an analytic shaped charge model or a hydrocode calculation. The calculation which provides V_l also provides the jet tip velocity, thus allowing the determination of the maximum coherent jet tip velocity.

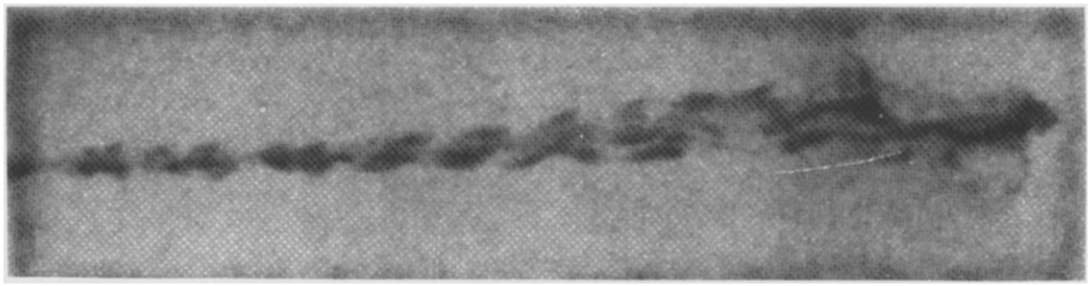

Fig. 2. X-ray view of the jet from an aluminum 20° liner angle charge.

More direct, however, is another expression used for jet coherency:

$$V_{jet\ tip} \leq 2.41 c_0 \tag{3}$$

This expression (Walters and Zukas, 1989) more simply states that the maximum jet tip velocity is 2.41 times the bulk sound speed of the liner material, and thus combines effects of high pressure and charge geometry into one constant. (Chanteret, 1992, suggests 2.46 rather than 2.41, and that even higher jet tip velocities are possible depending on the actual geometry and explosive of the charge.) Although further removed from physical meaning, Eq. (3) is also based on empirical results, and in Table I it is used to estimate the maximum tip velocity for various materials. The last column lists coherent jet tip velocities observed for the materials: the aluminum value is from this research, and all other values are from Chanteret (1992).

Table I. Coherent Jet Tip Velocities

Material	Bulk Sound Speed (km/s)	Maximum Coherent Jet Tip Velocity (From Eq. 3) (km/s)	Observed Coherent Jet Tip Velocity (km/s)
Aluminum	5.35	12.9	11.5
Copper	3.94	9.50	9.7
Molybdenum	5.12	12.3	12.3
Nickel	4.60	11.1	11.4
Steel	4.57	11.0	10.7 (Iron)

Aluminum is the most common structural material for satellites. Although density estimates for space debris are debris size dependent (NASA, 1991), estimates usually place it near that of aluminum. According to Eq. (3), it should be possible to design a charge which would produce a coherent aluminum jet tip travelling at 12.9 km/s. For a conical charge with an aluminum liner, it is possible to plot the jet tip velocity versus liner angle. This is done for the Octol 70/30 explosive in Fig. 3, using the SC1d model (Buckley, 1990). In our experiments using an Octol 70/30 explosive and conical aluminum liners, a 30° liner angle produced a coherent jet travelling at 11.2 km/s, while a 20° liner angle produced an incoherent jet travelling at 12.0 km/s. The fact that aluminum does not seem to follow Eq. (3) has been noted by other researchers (Chanteret, 1992), and experimentally it appears that the fastest coherent jet possible with aluminum has a jet tip velocity less than 11.6 km/s. Equation (3) does appear to hold for other materials, and the corresponding coherent jet tip velocities for many other materials have been achieved. Thus, the technique described in this report should be applicable to the hypervelocity launching of fragments of other materials.

EXPERIMENTAL PROGRAM

The hypervelocity fragment launcher design was based on an aluminum lined conical shaped charge, shown in Fig. 4. As discussed above, initial experiments showed that a 20° liner angle did not produce a coherent jet. Therefore, 30° liner angle charges were examined in tests and computations (Grosch, *et al.*, 1991, and this research). Early tests used the cup shaped apex depicted in Fig. 4. The cup shaped apex was initially adopted since Kronman and Merendino (1963) has used such a design. It was thought that a larger jet tip might be produced by such an apex. More recent tests utilize a hemispherical apex, which produces a more repeatable jet tip. The liner was made of 1100-O aluminum. The explosive was Octol 70/30, and was initiated by an RDX booster pellet at the top of the charge. The charge height was 15.75 cm, and the charge diameter was 6.5 cm.

Tests were performed both in atmosphere and in an evacuated chamber. In the tests, the dimensions of the inhibitor were varied. Two pair of orthogonal flash X-rays were used to image the jet in flight. These radiographs were used to determine the influence of changes in the inhibitor on the jet tip. The craters resulting from the impact of the jet with aluminum targets were also studied. For the tests in atmosphere, the standoff from the target was 110 cm, and X-ray heads were centered at 41 cm and 92 cm from the base of the charge along the flight line. For the tests in the evacuated chamber, the standoff from the target was 271 cm, and X-ray heads were centered at 203 cm and 251 cm from the base of the charge along the flight line. Tests in the evacuated chamber were performed at a pressure of 3 torr. Jet tip velocities were obtained from location measurements on the X-ray radiographs. The jet tip velocities were very repeatable, with a jet tip velocity of 11.2±0.2 km/s.

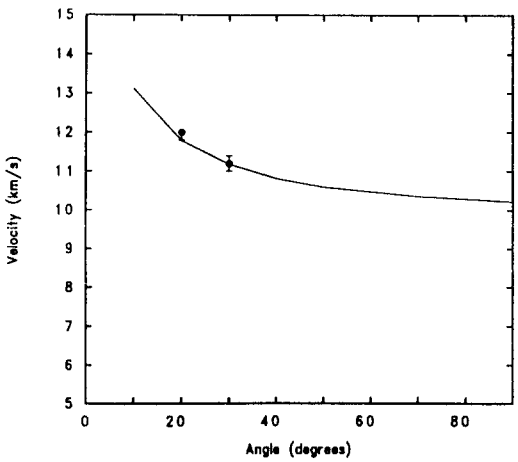

Fig. 3. Jet tip velocity versus liner angle, based on a one-dimensional shaped charge model. The dots are experimental values.

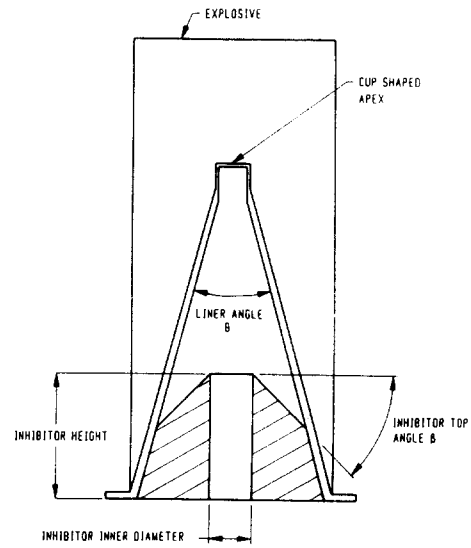

Fig. 4. The shaped charge and inhibitor set-up and terminology.

In early testing, flash radiographs revealed that when a fragment exited the charge, it was followed by trailing debris. This debris was unlike the fragments following the jet tip seen in Fig. 1, in that the particles were smaller and were spread over a larger region. The inhibitor removed most of the jet, but additional trailing debris exited the charge. The computational results were therefore carefully examined to gain a greater understanding of jet formation and inhibitor interaction to suggest an approach for removing this trailing debris.

COMPUTATIONS

A series of computations modeled the shaped charge jet formation (Walker, 1991). These were done concurrently with experiments, and were used to aid in the interpretation of experiments and suggest further refinements in the inhibitor design. Interestingly, the experimental results also aided in the interpretation of the computations. Lagrangian calculations were performed with the hydrocode EPIC (Johnson and Stryk, 1986) and Arbitrary Lagrangian-Eulerian calculations were performed with the hydrocode CALE (Tipton, 1990). The liner and inhibitor were modeled as elastic-perfectly plastic, with relatively low flow stresses, and with a Mie-Grueneisen equation of state. The explosive was modeled with the JWL equation of state, with a detonation velocity of 8.48 km/s. The collapse process was modeled in detail, as was the inhibitor response. There were three primary results of the computations:

1) It was determined that the inhibitor should be made of a dense material, instead of the low density plastic used previously (Kronman and Merendino, 1963). Subsequently, copper was used in testing.

2) It was revealed that the inhibitor collapse was not actually cutting the jet. Rather, the inhibitor was pinching down on the jet, causing the portion of the jet already formed to stretch and fragment. This isolated the jet tip as a large fragment, but also created the debris immediately following it. This understanding of the origin of the debris suggested techniques for its removal.

3) The computations provided information on jet material's original location in the liner, as well as the path this material was traversing as it travelled from the liner to the collapse region, and into the jet. The material's path (location versus time) was helpful in determining the geometric arrangement of the inhibitor and the asymmetric insert placed within the charge cavity. The computations identified which material in the liner needed to be given an off-axis velocity component, and where the insert should be located to provide it.

Each of these results would have been very difficult to obtain experimentally, as it would have taken extensive testing and the use of X-ray techniques for looking inside the liner and inhibitor during the collapse. Each will be discussed in more detail below. Also, calculations were performed with both cup and hemispherical apexes to verify that inhibitor geometry did not need to be altered due to the change in apex design.

Lagrangian Calculations

The intent of early calculations was to determine the appropriate size and shape for the inhibitor. Different heights and materials for the inhibitor were examined. The major result of the Lagrangian computations was that a more dense material should be used for the inhibitor. In the early work (Kronman and Merendino, 1963) a plastic had been used. However, in the computations this material was ineffectual in cutting the jet. Calculations with inhibitors made of various materials convinced us that material inertia is more important than strength in cutting the jet. In the present design, the inhibitor is made of copper, a relatively dense material.

Calculations were also done to investigate inhibitor heights and shapes. Three different top designs were examined: these included a flat top ($\beta = 0$) and tops with angles $\beta = \pm 45°$ (see Fig. 4). In the EPIC computations, the resulting jet after pinching was the most narrow for the +45° slope. This design was adopted.

Due to the way jet collapse occurs, it was not possible to sever the jet computationally. Based on observed collisions between and jet and inhibitor, and the subsequent narrowing of the jet, it was possible to infer where cutting would probably occur. This is an underlying difficulty in the Lagrangian calculations, since the cutting of the jet to produce a single fragment was the program objective. To learn more from computations, it was necessary to transition to an Eulerian formulation. It was thought such an approach would allow the examination of the separation of the jet material to form a fragment. However, the jet tip separation process is quite complicated, and even Eulerian formulations were not be able to treat the fragmentation which occurs. Thus, inferences regarding the formation of the fragment were still necessary.

Arbitrary Lagrangian-Eulerian Calculations

Arbitrary Lagrangian-Eulerian (ALE) codes allow the grid motion to be independent of the material motion. If the grid is fixed, the calculation is purely Eulerian. If the grid moves with the material, the calculation is purely Lagrangian. ALE is between these two extremes. The grid has its own equations of motion, and the grid can move independently of the material motion or be linked to the material motion in some fashion.

In the ALE calculations, the zoning roughly moved with the jet material, making it possible to maintain fine zoning in the jet even though it was impractical to cover the entire region of interest with fine zoning. In this sense, the ALE approach was very beneficial. The ability of the material to move independent of the mesh (Eulerian) avoided very small zones due to the large deformations in the jet collapse. The ability of the mesh to loosely follow the material (Lagrangian) kept relatively fine zoning in the area of interest as the jet travelled along the flight line.

Severing of the Jet

The ALE calculations led to a (presumably) fairly accurate picture of what was happening during the liner collapse, and how the jet was being severed.

It was learned that the inhibitor was not cleanly cutting the jet. Rather, the jet was being "cut" in three steps. First, the initial part of the jet forms. The jet tip begins traveling down the axis of symmetry, through the hollow inner diameter of the inhibitor. Second, when the detonation front reaches the inhibitor, the inhibitor begins an inward radial collapse which clamps down on the jet. As the inhibitor is quite dense, this greatly decelerates the portion of the jet which comes in contact with the collapsing inhibitor. Third, a large velocity gradient in the jet results, where the jet tip, with a velocity of roughly 11 km/s, is traveling much faster than the portion of the jet trapped by the inhibitor. A region of the jet between the jet tip and the top of the inhibitor then stretches and fragments. The jet tip survives as a large fragment, and numerous small trailing fragments are created.

This sequence of events can be seen in Figs. 5, 6, and 7. Figure 5 shows the initial geometry comprised of an aluminum liner and a copper inhibitor with 5.08 cm height and 1.19 cm inner diameter, an aluminum base plate on which the charge rests with a 1.27 cm hole, as well as a steel supporting structure. The cavity is filled with air. Figure 6 is a sequence of material boundary plots from the collapse, from 8 μs to 19 μs. By 10 μs, the jet tip is formed. The "wing-tip" shape of the jet tip is due to the cup shaped apex of the liner — it does not occur for a hemispherical or conical apex. During this early collapse, the aluminum's trip from its original liner location (measured from the time of arrival of the detonation front) to the jet takes roughly 4 μs. By the time it reaches the jet, the aluminum has been plastically strained nearly 400%. This corresponds to plastic strain rates on the order of 10^6 s^{-1} (4/4 μs = 10^6 s^{-1}). At 15 μs, a section of the collapsing liner collides with the top of the inhibitor ($\beta = +45°$), almost simultaneously along the whole top of the inhibitor. This collision behavior is part of the reason the slanted $\beta = +45°$ top was chosen. The explosive now begins driving the inhibitor closed, and liner material touching the inhibitor nearly comes to a stop due to the density and volume of the inhibitor. At 16 μs, the top of the inhibitor begins to collapse, and by 19 μs it is clamping down on the jet.

Between 16 μs and 19 μs, the jet tip travels 3.4 cm, which gives it a velocity of 11.3 km/s. The front 3 cm of the jet has passed by the top of the inhibitor before the collision between the inhibitor and the liner, and now appears to travel without alteration in shape. The jet material between the jet tip and the inhibitor is undergoing large tensile deformations. Plastic strain rates in this region of the jet are between 10^5 s^{-1} and 10^6 s^{-1}. This large stretching tears the jet apart. To see this, consider the upper half of the sequence in Fig. 7, which is a density plot for a different computation (the lower half of the figure will be discussed in the next section). At 15 μs (Fig. 7d) the collision with the inhibitor has just occurred and the jet has not yet begun to stretch. The density throughout the jet is uniform. At 16.5 μs (Fig. 7e) the jet has begun to stretch, and in the density plot the decrease in density is the darker region within the jet. At 20 μs (Fig. 7f) the region of the jet between the inhibitor and the intact jet tip has a low density, implying material separation.

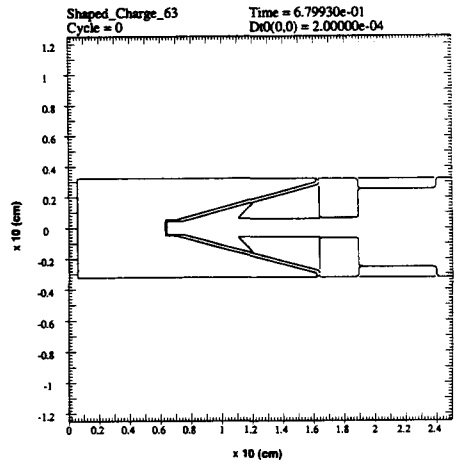

Fig. 5. Initial geometry showing liner, copper inhibitor, aluminum plate, and steel support.

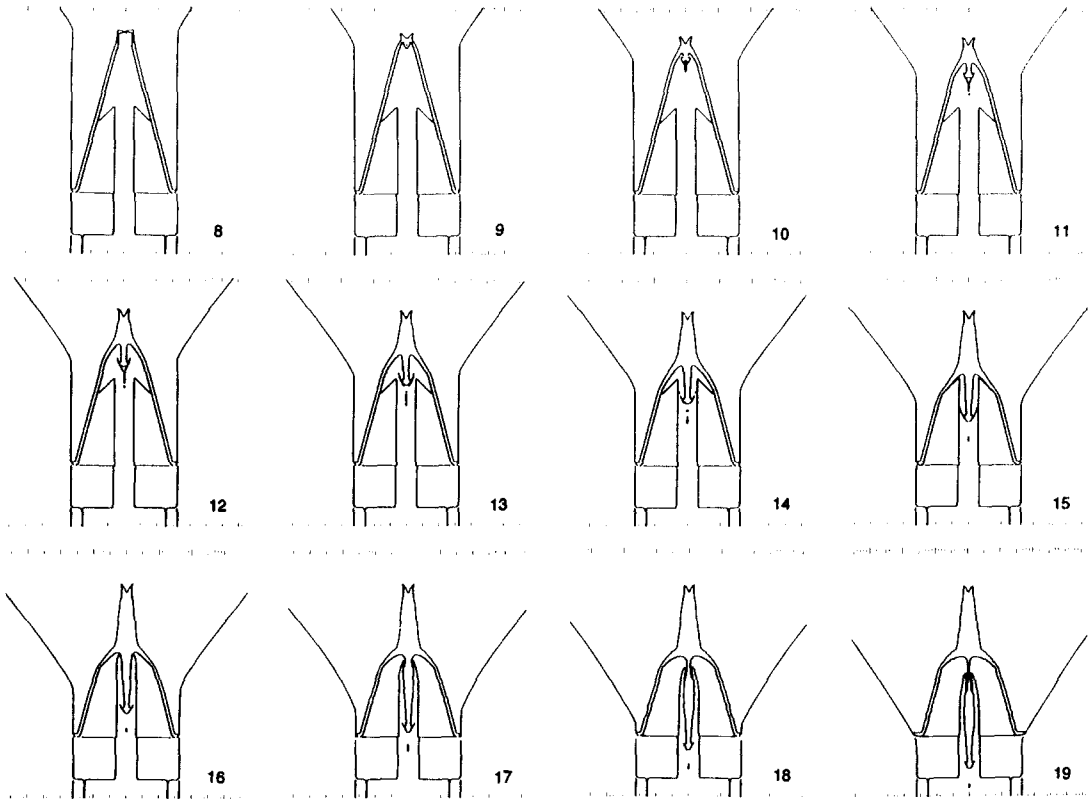

Fig. 6. Sequence of frames showing the collapse of liner and interaction with inhibitor at 8 μs to 19 μs.

In the calculations, this region continues to stretch, as there is no mechanism in the computer code for fracture of the material. However, in the actual physical event, the large tensile stresses cause the jet material to fracture and fragment. The front region of the jet is nearly unaffected by this fragmentation, forming the desired large fragment, but the region with the large tensile gradient breaks into pieces. These pieces form a debris cloud, which follows the main fragment. For a clean fragment, this debris must be removed.

The Sliced Liner Calculations

To overcome some of the difficulties in eliminating trailing debris in the tests, a better understanding of the jet material's original location in the liner was needed. Following Walters and Golaski (1987), the aluminum liner was sliced into pieces of width 0.5 cm. Each slice was identified in the code as a differenct region, making it possible to follow each slice of the liner separately throughout the calculation.

Six different times from the calculation with a sliced 30° liner are shown in Fig. 7. The upper half of each figure is a density plot, with the grey scale to the right indicating density. The initial densities of aluminum (2.70 g/cm^3) and copper (8.93 g/cm^3) have been identified. At the center of collapse, where pressures are slightly above 0.5 Mbar, the aluminum has been compressed to a density of 3.6 g/cm^3. This region is often referred to as a stagnation point, because material remains there on the dividing line between flow into the jet and flow in the opposite direction into the slug. The lower half of each figure shows the region shading. In the original work, each slice was colored, but in this paper the figures have been reproduced in black and white. The aluminum liner is represented by five shades for each of five different regions.

In Fig. 7b (10 μs) the detonation front in the explosive is marked, and is discernable in the density plot by a slight compression. The pointed tip of the jet is being formed by the top of the cup shaped apex. The cavity in the jet tip and the subsequent wing tip front on the jet are due to the cup shape of the apex, not the slicing of the liner. Figure 7c (12.5 μs) shows that most of the liner material is going into the slug; one-tenth to one-fifth of the liner material goes into the jet. Figure 7d (15 μs) shows the collision of the liner and inhibitor. Almost all the material from the cup apex has been left behind. The jet tip is comprised of material from the liner near the intersection of the cup and the cone. The first 3 cm of the jet comes from inner surface material of the first 7 slices of the liner (not counting the two at the apex), or about 3.5 cm of liner material. If the liner were conical all the way to the apex, this would be 4.6 cm of liner material. Thus, the liner material which makes up the jet tip has been identified.

The copper inhibitor is pressing into the collapse point in Fig. 7e (16.5 μs). Material in the 8th slice of the liner ends up in the tail end of the jet. The density plot reveals that the jet density near the inhibitor is beginning to decrease, indicating that the material is stretching. At this stage, fragmentation probably begins. Figure 7f (20 μs) shows that a large length of the jet has low density, implying that it has undergone large tensile stretching. However, the tip of the jet is moving with little deformation. The jet tip is composed of material from the first four or five slices of the

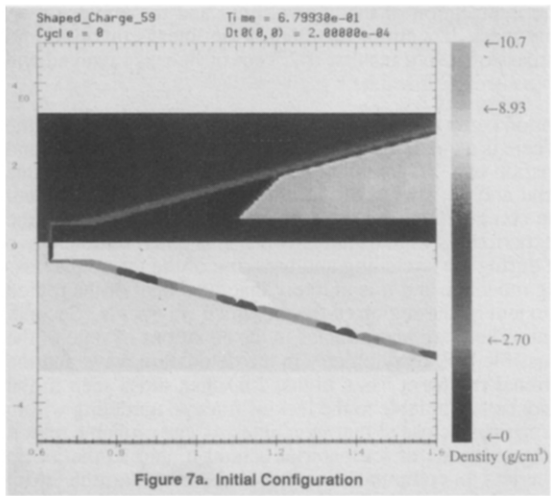

Figure 7a. Initial Configuration

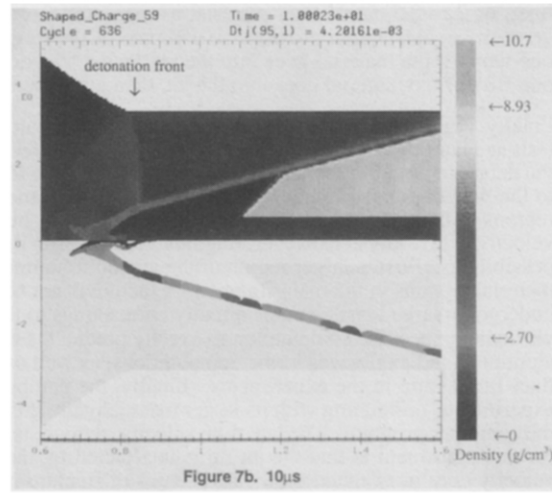

Figure 7b. 10μs

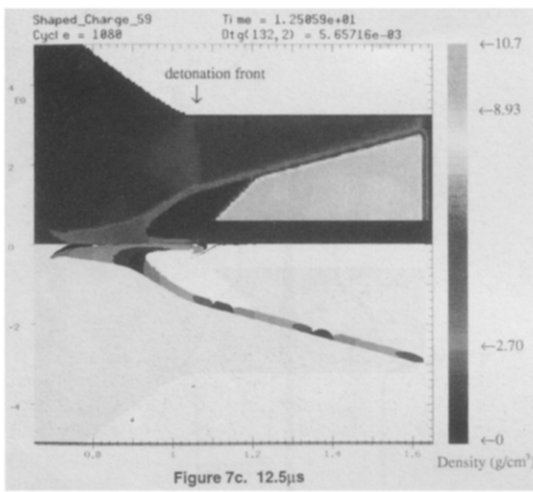

Figure 7c. 12.5μs

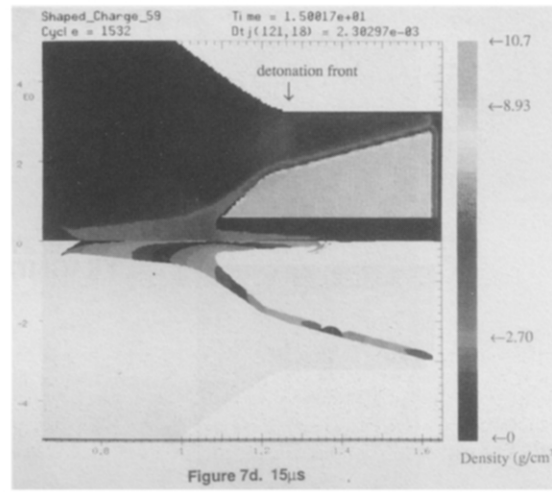

Figure 7d. 15μs

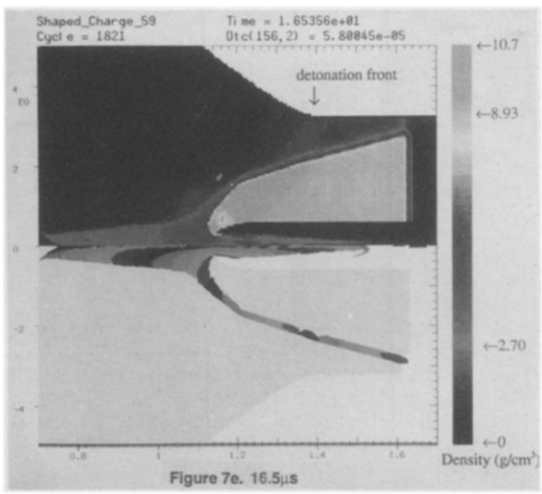

Figure 7e. 16.5μs

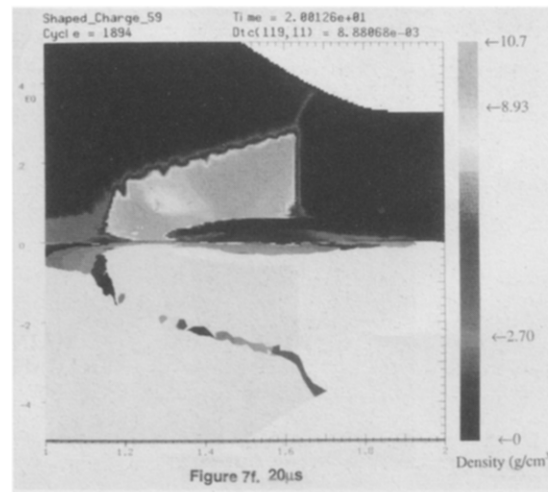

Figure 7f. 20μs

Fig. 7. Sequence of frames showing the interaction of the jet and the inhibitor.

liner, or 2 to 2.5 cm of liner material as measured from the intersection of the conical liner and the cup apex. A geometrical calculation provides an estimate of the fragment mass: if 2 cm of material of the liner is involved and one-tenth of the material goes into the jet, then a fragment mass of 0.96 g results; if 2.5 cm of liner is involved and one-fifth of the material goes into the jet, then a fragment mass of 2.52 g results.

Finally, Fig. 8 (40 μs) is a late time picture from this calculation compared with an X-ray radiograph from one of the tests at a later time (65 μs), where the length scales differ. There is a qualitative agreement between the fragment and the debris in both the calculation and experiment. The formation of a "fragment" in the numerical calculation is due to the way the interface tracker preferentially moves material and the slicing of the liner providing many different regions to be moved: fracture is not being modeled. In the computation, the mass of the fragment is 1 g, and the velocity is 11.2 km/s. However, fragment masses from the experiments were usually lower. This could be due to two possibilities. First, a larger region of the jet could fragment during the stretching and breaking of the jet, so that less material remains in the main fragment. Fracture is not being modeled, and it is unlikely that the extent of the region undergoing large tensile strains directly corresponds to the extent of the region of the jet which fragments. Second, we do not expect the computation to exactly predict the event. There are inaccuracies in the equations of state of the aluminum and explosives in the computations, as well as possible lack of symmetry in the detonation wave and the liner fabrication in the experiments. Finally, the computational fragment has a higher L/D than those seen in the experiments, correlating with its larger mass. Again, this may be attributable to the lack of fracture modeling within the computer program. The late time velocity, though, is surprisingly close to that seen in tests. The probable reason for this agreement is that the jet tip is unaffected by the fragmentation of jet material behind it, and so the jet tip velocity does not depend on the mechanics of fracture of the jet. In computations without the inhibitor, the jet tip looks exactly the same as those computations which include an inhibitor. A copper jet is also seen in the calculations. Such a jet was not observed in the tests, although small amounts of copper did impact some of the targets.

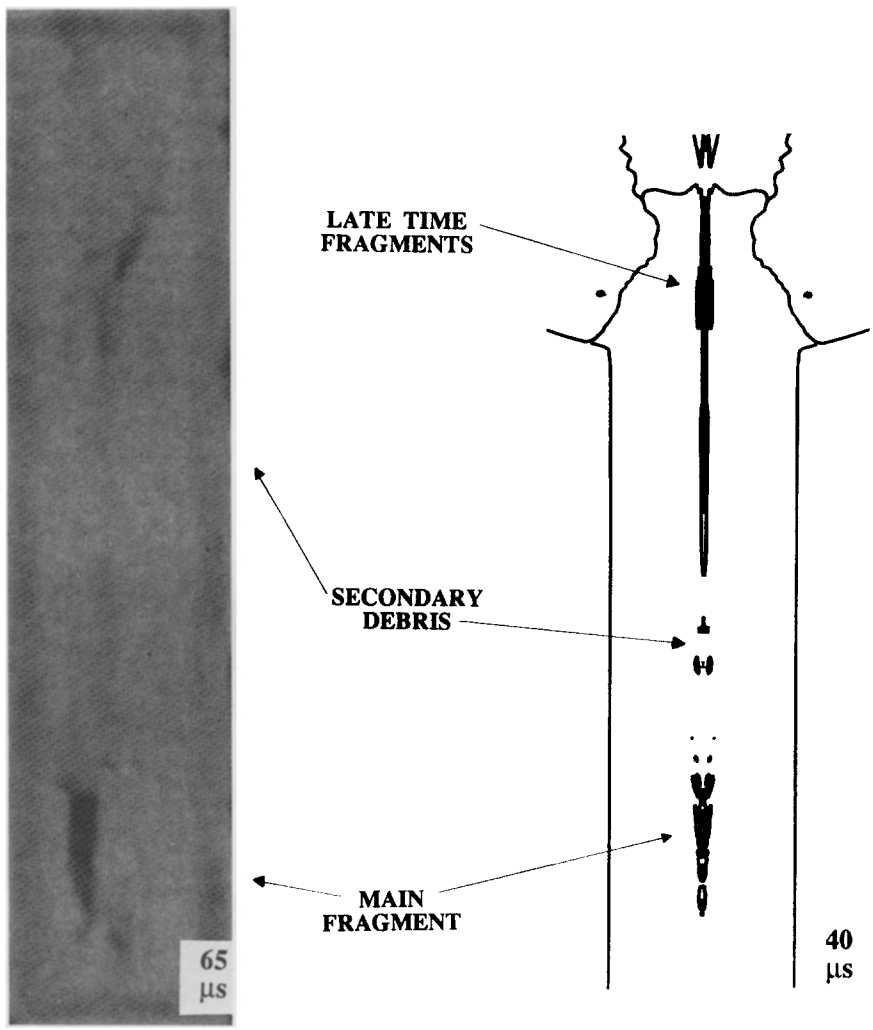

Fig. 8. Products produced by an inhibited shaped charge.

Removing the Trailing Debris

The jet severing interpretation provided by the computations and experiments showed that the trailing debris, which was coming from the stretching and breaking of the jet, could not be removed by altering the height or inner diameter of an axially symmetric inhibitor. To avoid active systems, such as explosive flyer plates, an asymmetry was needed in the collapse to push the debris off the flight line.

If the liner material which formed the debris was given an off-axis velocity component before it entered the collapse region, it would go through the jet formation and subsequent fragmentation process and still have an off-axis velocity component. Based on wave transit times, it appeared it would not be possible to produce the desired asymmetric behavior by applying a partial exterior confinement to the explosive. Rather, the asymmetric behavior would need to be caused by an insert within the cavity. The calculations were 2-D axisymmetric, but they could still be used to see if the location of the asymmetric insert allowed interaction with the liner material at the proper times and locations.

If the liner material that became the part of the jet which stretched and broke could be given an off-axis velocity, that debris would not impact the target. The sliced simulations identified the liner material that needed to be affected. Figure 7 shows that the region of liner material that goes into the stretching region of the jet begins in the 4th and 5th slices. Thus, only the first 2 cm of liner material should be allowed to collapse without being affected by the insert.

An asymmetric triangle insert was placed on top of the inhibitor. To check the timing of the design, a calculation was done with an aluminum tube inside the inhibitor, the tube having the same height as the triangle insert. Figure 9 shows the initial geometry, as well as two later times. At 12 μs, the liner is just impacting the insert. This material would be the first part of the liner to have an asymmetric collapse, and thus an off-axis velocity component. The next frame, at 13 μs, shows the progression of the interaction. Due to the symmetry of the calculation, a continuation of this calculation is not relevant to the jet behavior. However, this calculation does show that the insert allows the jet tip material to collapse unaffected to form the fragment.

Figure 10 is comprised of two radiographs. The one on the left is from a test without the asymmetric insert, while the one on the right has the insert. Otherwise, the two tests are identical. It appears the insert is removing the late time debris, and examination of the targets confirmed this conclusion.

EFFECTS OF THE ATMOSPHERE

In addition to tests in air, tests in vacuum were desired to more realistically test spacecraft shielding components. The transition from air to a vacuum resulted in some dimension changes for the inhibitor and insert. The figures so far presented have been from tests in air; the rest of the figures will be from tests in vacuum.

Air seemed to affect the fragment. Erosion of the jet tip was clearly visible in an uninhibited test where there was substantial rotation of the leading fragment. In another uninhibited test, the large particle at the jet tip was seen to decrease in length between radiographs, from 3.0 cm to 2.3 cm in 50 μs (over a distance of 57 cm). This could be due to a number of effects: a negative velocity gradient in the particle, which would contract the particle; mechanical erosion of one material travelling through another; and ablation, where a phase change aids in the erosion. As to a negative velocity gradient in the jet tip, no change in the jet tip diameter was detectable from the radiographs, and a negative velocity gradient in the jet tip was not observed in the computations. The second two possibilities are difficult to quantitatively discuss. If the materials were incompressible perfect (nonviscous) fluids, Bernoulli's law could be used to estimate the erosion rate:

$$\frac{1}{2}\rho_{Al}(v-u)^2=\frac{1}{2}\rho_{air}u^2 \qquad (5)$$

where v - u is the erosion rate. With ρ_{Al} = 2.7 g/cm^3 and ρ_{air} = 1.3 g/l one obtains an erosion rate of 250 m/s. In the above test, 1.25 cm would have eroded based on this approach. This is much larger than what actually occurred, but then air and aluminum are not incompressible perfect fluids, especially air at these velocities. However, certainly some decrease in length is due to erosion.

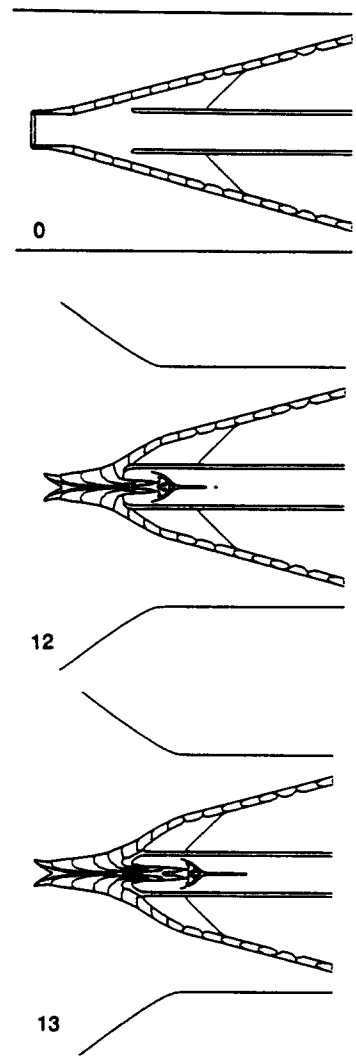

Fig. 9. Three times from the calculation with a tubular insert, at 0, 12, and 13 μs.

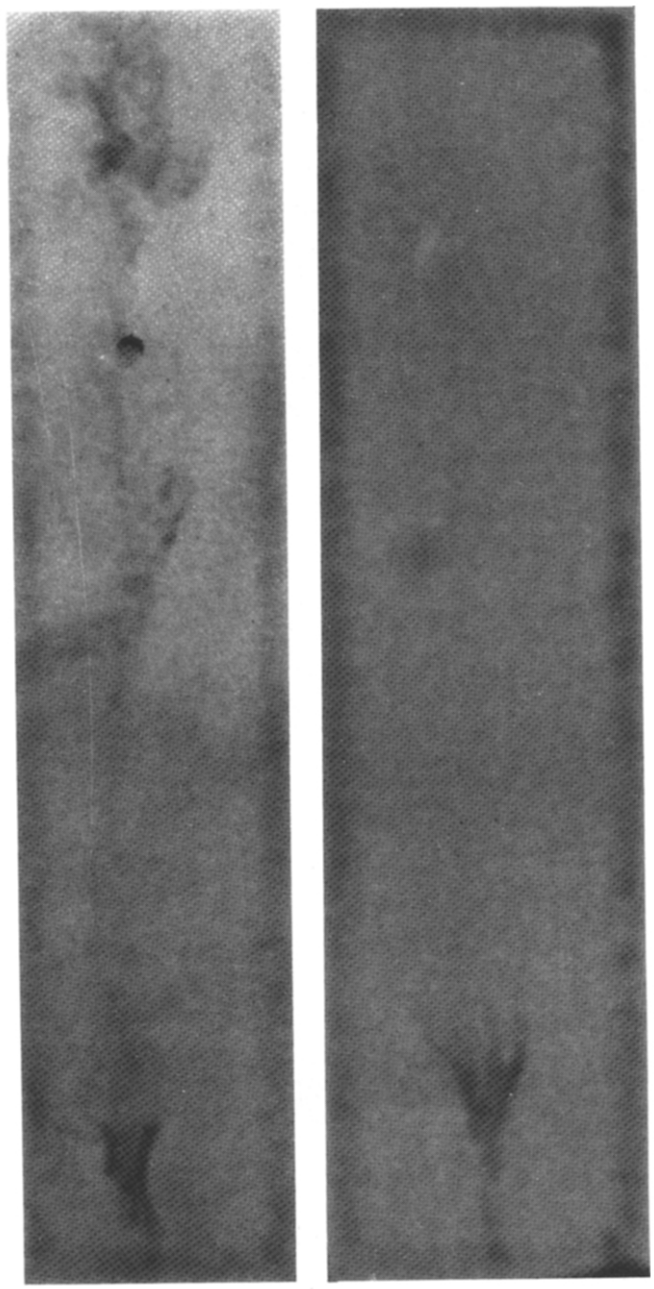

Fig. 10. X-ray views of tests without (left) and with (right) the aluminum insert. Note the absence of trailing debris in the right view.

Once in the vacuum chamber, the inhibitor and insert dimensions which were being used for the atmospheric tests produced an incohesive fragment over the greater flight distance. This was resolved by decreasing the height of the inhibitor, and lowering the height of the insert. This gave rise to a cohesive fragment with a larger mass. However, the fragment now seemed to be surrounded by a small amount of debris. It is possible that the air was helping retard this debris in the atmospheric tests.

EXAMPLES

The current design of the hypervelocity fragment launcher uses a copper inhibitor of height 4.47 cm and an inner diameter 1.19 cm, and a 0.76 cm tall triangular aluminum asymmetric insert placed within the cavity of the charge, shown in Fig. 11. These dimensions were determined through both experiments and computations. In the following X-ray views, the direction of motion is from top to bottom.

As a first example, Fig. 12 shows orthogonal views from the test which had the highest rotation rate encountered during the test program, rotating 90° in 240 μs. This rotation rate was constant based on measurements from the two sets of radiographs, with 0° extrapolating back to the vicinity of the original charge location. The fragment velocity was 11.1 km/s. These views showed that the fragment was hollow. Careful examination of Fig. 7 shows that the computations were also showing a decreased material density along the axial centerline.

Next, Fig. 13 shows orthogonal views of a fragment in flight. The fragment had an approximate length of 1.4 cm and a diameter of 0.53 cm to give an L/D of 2.6. Using a diameter for the hollow region of 0.18 cm, a fragment mass of 0.74 g was calculated. The fragment velocity was 11.2 km/s. The resulting crater in a 6061-T6 aluminum block is shown in Fig. 14. The target block was 15.3 cm in diameter, and 7.8 cm thick. The crater depth, measured from the top plane of the target, is 3.0 cm and its diameter is 4.1 cm. A spall plane is located 0.6 cm from the bottom of the target. The two very small craters visible on the top surface (to the right of the main crater) are due to trailing debris.

Although the charge is being used for the testing of shielding concepts at this time, it is still undergoing refinement.

CONCLUSION

The primary achievement of this program was the design of a hypervelocity fragment launcher. Experimental tests were performed to evaluate and refine the design. Numerical simulations were able to provide a qualitative picture of how the inhibitor was interacting with the jet, as well as quantitative times for these interactions. These computations provided considerable guidance in the design of the insert and inhibitor. The hypervelocity fragment launcher is being used to test various spacecraft shielding concepts. Further work would be to remove the remaining debris which seems to be travelling along with the fragment in the vacuum tests.

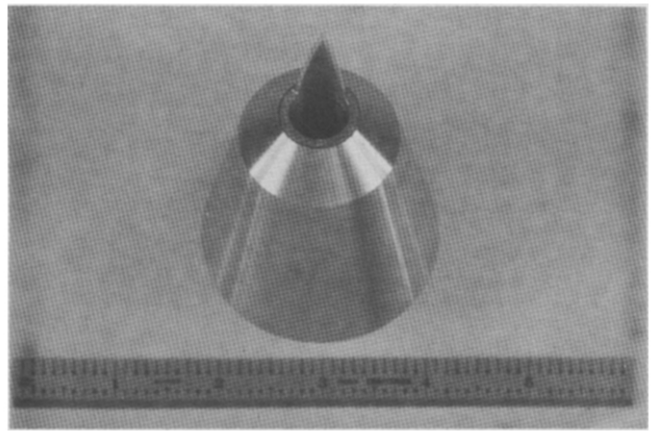

Fig. 11. Inhibitor design, with insert.

ACKNOWLEDGEMENTS

We would like to thank Jeanne Crews NASA-JSC for primary support and encouragement for this work. Support for calculations was also supplied by Southwest Research Institute under their Internal Research program. Robert Tipton and Chris Simonson, of Lawrence Livermore National Laboratories, were helpful in answering questions about CALE. The authors would like to thank Randy Tullos for his considerable help in all phases of the project.

REFERENCES

Buckley, P. (1990). Shaped Charge One-Dimensional (SC1d) computer code (evaluation copy), PMC, Inc.

Chanteret, P. Y. (1992). "Studies of Maximum Velocities for Coherent Shaped Charge Jets," *13th International Ballistics Symposium*, Stockholm, Sweden.

Grosch, D., J. Walker, S. Mullin and R. Tullos (1991). "Development of an Inhibited Explosive Hypervelocity Launcher," Southwest Research Institute Final Report 06-3513, San Antonio, Texas.

Johnson, G. R. and R. A. Stryk (1986). "User Instructions for the EPIC-2 Code," AFATL-TR-86-51.

Kronman, S. and A. Merendino (1963). "Inhibited Jet Charge," *Proceedings of the Sixth Symposium on Hypervelocity Impact*, Cleveland, Ohio.

Merendino, A., J. M. Regan and S. Kronman (1963). "A Method of Obtaining a Massive Hypervelocity Pellet From a Shaped Charge Jet," Ballistic Research Laboratories Memorandum Report No. 1508, Aberdeen Proving Ground, Maryland.

NASA (1991). "Space Station Program Natural Environment Definition for Design," Change Notice A1, SSP 30425 Revision A July 1991.

Tipton, R. (1990). "CALE Users Manual, Version 901101," Lawrence Livermore National Laboratory, Livermore, California.

Tullos, R., W. Gray and S. Mullin (1988). "Test and Evaluation of an Explosive Hypervelocity Launcher," Southwest Research Institute Final Report 06-1967, San Antonio, Texas.

Tullos, R., D. Grosch and J. Walker (1990). "An Explosive Hypervelocity Launcher for Orbital Debris Impact Simulations at 11.4—11.9 km/s," Southwest Research Institute Final Report 06-2880, San Antonio, Texas.

Walker, J. D. (1991). "Computational Modeling of an Explosive Hypervelocity Launcher," Southwest Research Institute Internal Research Report 06-9571, San Antonio, Texas.

Walters, W. P. and S. K. Golaski (1987). "Hemispherical and Conical Shaped-Charge Liner Collapse and Jet Formation," US Army Ballistic Research Laboratory Technical Report BRL-TR-2781, Aberdeen Proving Ground, Maryland.

Walters, W. P. and J. A. Zukas (1989). *Fundamentals of Shaped Charges*, New York, Wiley-Interscience.

Wenzel, A. B. (1987). "A Review of Explosive Accelerators for Hypervelocity Impact," Int. J. Impact Engng. 5, 681-692.

Wenzel, A. B. and J. W. Gehring (1965). "Techniques for Launching 0.01- to 25-Gram Discrete Projectiles at Velocities Up to 54,100 Ft/Sec," *Fourth Hypervelocity Techniques Symposium*, Arnold Air Force Station.

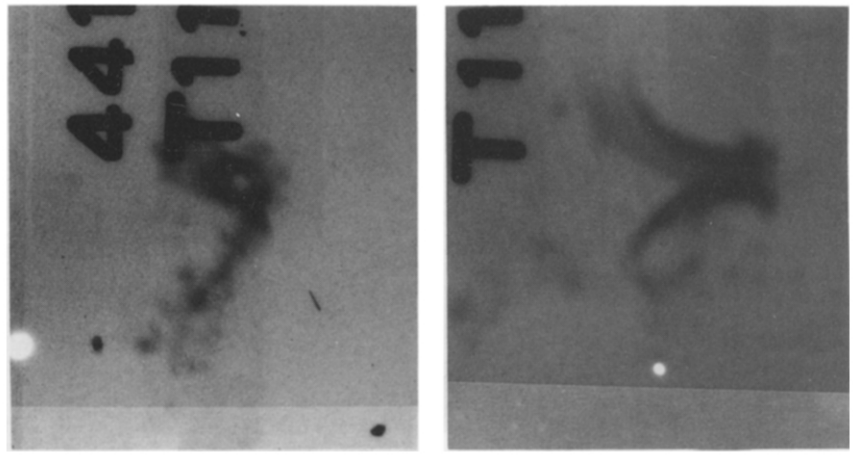

Fig. 12. Orthogonal radiographs of rotating fragment, travelling at 11.1 km/s.

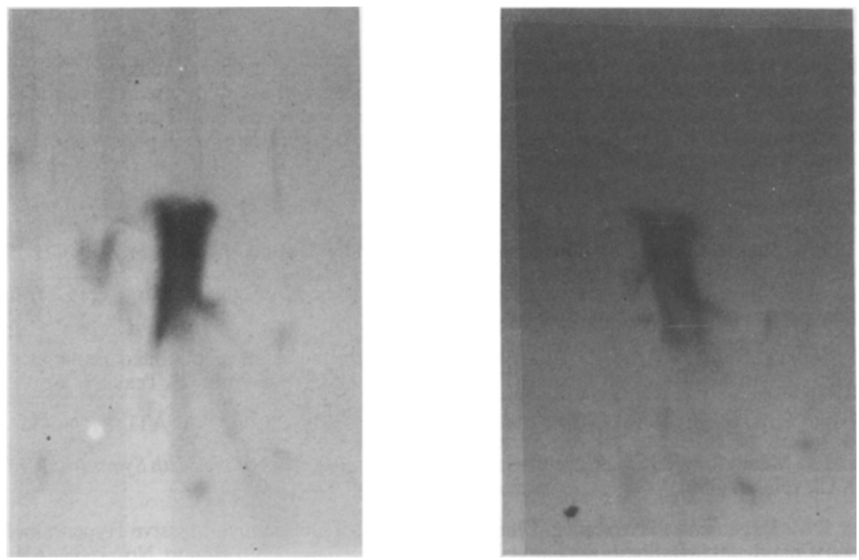

Fig. 13. Orthogonal radiographs of fragment travelling at 11.2 km/s.

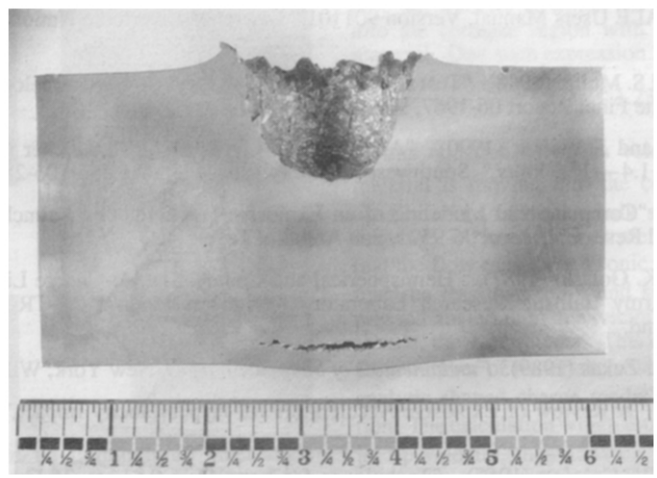

Fig. 14. Photograph of crater resulting from impact of Al 6061-T6 target and fragment shown in Fig. 13.